Molecular dynamics study of nanobubbles in the equilibrium Lennard-Jones fluid

D. I. Zhukhovitskii[1, a)]

Joint Institute of High Temperatures, Russian Academy of Sciences, Izhorskaya 13, Bd. 2, 125412 Moscow, Russia

(Dated: 23 November 2014)

We employ a model, in which the density fluctuations in a bulk liquid are represented as presence of the clusters of molecules with the lowered number of nearest neighbors (number of bonds). The nanobubble size distribution is calculated on the basis of a close analogy between the surface part of the work of formation for a cluster and for a nanobubble. The pre-exponential factor for this distribution is related to the fluid compressibility. Estimates made for different liquids show that it can be noticeably different from that adopted in the classical nucleation theory (CNT). Molecular dynamics (MD) simulation is performed for a liquid inside a macroscopic droplet of molecules interacting via the Lennard-Jones potential plus a long-range tail. The nanobubbles are identified by clusters of bond-deficient particles with the optimum number of bonds that provide the maximum nanobubble number density and maximum resolvable nanobubble equimolar size. The results of MD simulation are in qualitatively better agreement with proposed theory than with CNT.

PACS numbers: 64.60.Q-, 62.10.+s, 61.25.Em, 64.60.Q-

[a)]Electronic mail: dmr@ihed.ras.ru; http://oivtran.ru/dmr/

I. INTRODUCTION

The classical nucleation theory (CNT) is a universal method for investigation of kinetics of the first-order phase transitions[1–5], in particular, of the bubble nucleation in liquids[6,7]. In some cases of practical interest, the embryos of vapor phase spontaneously emerging in a metastable liquid have extremely small sizes down to the intermolecular spacing. Such small embryo sizes are typical for the conditions of high superheats of liquids or for a stretched liquid under great negative pressure at relatively low temperature. This situation takes place in such phenomena as explosive boiling[8], sonochemistry[9], and cavitation erosion[10]; it can be encountered in operation of devices[11]. In the shockwave experiments, a liquid was first subject to compression and then, to stretch in the rarefaction wave[12–14]. Observed spallation of a liquid can be accounted for by nucleation of bubbles of extremely small sizes. Similar phenomena were registered upon spallation in laser shock-loaded tin in solid and liquid states[15] and in material decomposition upon femtosecond laser ablation[16].

Interpretation of experimentally observed nucleation rates on the basis of CNT leads in some cases to a reasonable agreement with experiment but in most cases, it mismatches the nucleation rate by ten orders of magnitude and even more. A reason for such discrepancy is the notion of a macroscopic liquid drop or macroscopic bubble involved in CNT. Obviously, both models are inappropriate for nanoscale objects. Because the nucleation rate is largely defined by the work of embryo formation, one can conclude that the size correction to this quantity is significant. Zeng and Oxtoby[17] and Oxtoby, Talanquer, and Laaksonen[18] have improved CNT by calculation of the size correction to the surface free energy of a droplet. Since these studies, a considerable efforts have been made to attain a good correlation between theory and experiment[19]. Modern theories (see, e.g., Refs. 20–31) are successful in interpretation of the vapor nucleation but less successful as applied to the bubble nucleation. A probable reason could be a worse convergence of the expansion for bubble work of formation in powers of the inverse bubble radius as compared to similar expansion for clusters. Hence in most of studies, the Tolman correction to the surface tension[32] is combined with CNT to provide a quantitative reproduction of experimental data. However, the resulting Tolman lengths (considered as an adjustable parameter) are incompatible with those required for interpretation of the vapor nucleation for the same substances.

The following theory extensions are worth mentioning. Deryagin, Prokhorov, and

Tunitskii[24] and Alekseechkin[25] have investigated the equilibrium distribution of bubbles in two-dimensional phase space (the size of a bubble and pressure inside it or the density) and calculated the correction to Zeldovich factor due to pressure (density) fluctuations. Yamamoto and Ohnishi[26] treated bubble nucleation in a binary solution of noble gases. Bubble formation in confined systems (pores) were studied by Neimark and Vishnyakov[27]; Glavatskiy, Reguera, and Bedeaux[28] have demonstrated that bubble formation in a confined system requires finite liquid compressibility. Note that it was shown by Reiss, Kegel, and Katz[29] that taking into account the finite compressibility removes translational redundancies, which lead to substantial increase of the pre-exponential factor in cluster equilibrium distribution over sizes. Iwamatsu[30] and Uline, Torabi, and Corti[31] used the density functional theory (DFT) to formulate such scaling rules of critical bubble quantities, which make scaled variables nearly temperature independent.

Numerical study of liquids seems to be the most plausible method for investigation of nanoscale bubbles (nanobubbles). Such simulation was performed in a number of studies for stretched liquids at the negative pressures up to the point of spallation. Thus, Corti, Debenedetti, Sastry, and Stillinger[33] performed Monte Carlo (MC) simulation of a superheated Lennard-Jones fluid and obtained the void-size distributions for the liquid-state configurations themselves and for their inherent structures. In MC simulation of the bubble nucleation, Kusaka and Oxtoby[34] proposed to characterize it by the number of molecules and interaction potential playing the role of order parameters. Meadley and Escobedo[35] performed MC simulation of bubble nucleation and obtained the kinetic rate for the Lennard-Jones system. Formation of a drop in the Lennard-Jones binary mixture and the critical behavior of the size correction to surface tension was investigated by Das and Binder[36].

In other studies, metastable fluids were studied using molecular dynamics (MD). Baidakov and Protsenko[37] and Baidakov, Bobrov, and Teterin[38] studied the Lennard-Jones fluid at a great negative pressure. Wang, Valeriani, and Frenkel[39] investigated the effect of local hot spots on the rate of bubble nucleation. Bazhirov, Norman and Stegailov[40] modeled cavitation in liquid metals under negative pressures and Kuksin, Norman, Pisarev, Stegailov, and Yanilkin[41] studied dynamics of spallation of the Lennard-Jones fluid. Recently, Abascal, Gonzalez, Aragones, and Valeriani[42], have reported the results of MD study of homogeneous bubble nucleation in water at negative pressure.

Microscopic cavities in a liquid at equilibrium and in superheated states were investi-

gated by Mountain[43] using MD simulation. MC simulations was performed by Huang and Chandler[44] to study cavity formation in the Lennard-Jones fluid at equilibrium. In both studies, the size distributions of cavities were obtained. Park, Weng, and Tien[45] obtained the size dependences of the surface tension and Tolman length by MD simulation of an equilibrium Lennard-Jones system with a bubble stabilized by fixed number of system particles.

In this study, we focus on the investigation of unstable nanoscale bubbles in an equilibrium liquid with equimolar sizes ranging from zero to several tens of molecules removed from the liquid. A correct statistical description of nanobubbles is crucial for development of a kinetic theory of bubble nucleation at great negative pressures, when the size of a critical nanobubble is very small. The scope of this paper is to obtain the data that could serve as a benchmark test for the size correction to a theory describing the size distribution of nanobubbles. A model proposed to account for the data obtained in MD simulation is similar to the cluster model[46,47], where the molecules that comprise the cluster are divided in the internal and surface ones; the latter form a monolayer on top of the former. This is also true for a flat liquid-vapor interface. Our model of a bulk liquid implies that a small admixture of surface molecules are locally present in the bulk thus forming the density fluctuations, which we call the nanobubbles. As the equimolar size of such nanobubble increases, an obviously detectable empty space emerges in its center, which leads to formation of a macroscopic bubble. A theory is based on a close analogy between the structure of the cluster and bubble surface. This allows one to use the same expression for the surface part of the work of nanobubble formation as for the cluster. On the basis of the work of nanobubble formation obtained in this way in Ref. 48, we deduce the nanobubble size distribution. Assuming that nanobubbles with sizes less than unity (density fluctuations) are responsible for fluctuation of the number of particles in given volume, we express the pre-exponential factor in their size distribution in terms of the liquid compressibility. This allows one to compare directly theoretical estimations with the results of MD simulation. It is noteworthy that, albeit proposed theory is not a "first principle" one, it includes no adjustable parameter.

The MD simulation was performed for the equilibrium Lennard-Jones fluid at the saturation curve and at high positive pressure to explore the validity of theoretical estimations in a wide range of state parameters. In addition to the short-range interaction, the particles are assumed to interact via the long-range gravitational-like potential[49]. In this study, a macroscopic droplet at equilibrium with surrounding vapor [the (P, T)-ensemble method[50]]

was used as a simulation system. A real system under investigation is a bulk liquid inside the droplet. This method of MD simulations has several advantages as compared to a common simulation ensemble in a rectangular box with periodic boundary conditions. Thus, the effect of the boundary conditions is absent, the simulation ensemble is not isochoric but isobaric, which removes a constraint for the fluctuation of number of particles. In addition, the pressure in the vicinity of droplet center is easily controlled by variation of the long-interaction coupling constant.

Identification of nanobubbles in a bulk liquid is a separate problem. In Ref. 33, it was proposed to use the Voronoi tessellation for this purpose; this method was also employed in Ref. 42. A search for the local regions with lowered internal energy was used in Ref. 41. We follow the idea of Ref. 39 to isolate spatial regions with lowered number of nearest neighbors (we term a bond the presence of a nearest neighbor), yet we have to refine this definition by specification of the maximum number of bonds for the bond-deficient particles. The latter is selected from competing considerations that the resulting number densities of nanobubbles reach maximum and, at the same time, the maximum resolvable nanobubble equimolar size is as large as possible. If we choose such optimum number of bonds, we avoid system-spanning nanobubbles, which are incompatible with the nanobubble size distribution independent on the size of simulation system at equilibrium. MD results show that such bond-deficient particles tend to clusterize thus forming clusters of particles with low number of bonds (bond-deficient clusters) that are quite similar to the lightest clusters in a vapor. To juxtapose theory and MD simulation results, we first calculate the equimolar size for each cluster that comprise k bond-deficient particles and then we plot the nanobubble number density against their equimolar size g. A reasonable agreement is demonstrated for both the fluid at saturation curve and the compressed fluid thus illustrating suitability of our approach.

The paper is organized as follows. In Sec. II, we write down the size distribution for nanobubbles of an arbitrary size based on the analogy with small clusters; in Sec. III, we analyze the fluctuation of the number of molecules in the system to deduce the pre-exponential factor in this distribution. In Sec. IV, the method of numerical simulation including nanobubble identification is discussed; MD simulation results are presented and compared with theory in Sec. V. The paper ends with a discussion of results and future directions (Sec. VI).

II. EQUILIBRIUM DISTRIBUTION OF ARBITRARY SIZE BUBBLES

In this Section, we will formulate the model of an arbitrary size nanobubbles in a liquid on the basis of a model of clusters in dense vapors[46,47]. In this paper, we confine ourselves to the treatment of a system in the state of thermodynamic equilibrium. It was shown in Ref. 47 that in the gas of Lennard–Jones molecules at temperature typically higher than melting one, microscopic clusters undergo a structural transition that transforms them into a set of virtual chains with the minimum number of bonds. Evaluation of the partition functions of such chainlike clusters leads to their size distribution

$$n_g = n_1 \exp\left(-\frac{\Delta\Phi_c}{T}\right), \quad \Delta\Phi_c = \frac{8\pi\sigma_\infty r_\ell^2}{3(\lambda+2\delta)}(g-1), \tag{1}$$

where $\Delta\Phi_c$ is the work of formation of a cluster comprising g molecules; n_g and n_1 are the number density of g-molecular clusters and monomers, respectively; T is the temperature (we use the energy units, $k_B = 1$); σ_∞ is the surface tension of a flat liquid–vapor interface; $r_\ell = (3/4\pi n_\ell)^{1/3}$ is the radius of molecular cell in a liquid, n_ℓ is the molecule number density in a liquid; λr_ℓ is the thickness of the cluster surface layer, δr_ℓ is the Tolman length; λ and δ are related to the dimmer equilibrium constant $K_2(T) = n_1^2/n_2$ and the number density of monomers at the saturation curve $n_{1s}(T)$ as

$$\lambda + 2\delta = \frac{8\pi}{3}\frac{\sigma_\infty r_\ell^2}{T}\ln^{-1}\frac{K_2}{n_{1s}}. \tag{2}$$

In the opposite limit of a large cluster, a relevant model is the classical drop model[1,2,19], in which the work of cluster formation is

$$\Delta\Phi_c = 4\pi\sigma_\infty r_\ell^2 g^{2/3} - (g-1)T\ln\frac{n_1}{n_{1s}}. \tag{3}$$

Distributions defined by (1) and (3) can be unified if we assume that an arbitrary-size cluster consists of a nucleus of $g - g_0$ internal molecules, whose state is very close to that in a bulk liquid, covered by a monolayer of g_0 surface molecules, which are in a different state characterized by pronounced bond deficiency. This model is vindicated by the bimodal distribution of molecules over the number of bonds found in Ref. 51. The layer of surface molecules is considerably perturbed by thermal fluctuations. However, it was demonstrated that instead of a real surface layer one could treat an effective one consisting of molecules with any preassigned number of bonds, average density of surface molecules, and thickness.

Consideration of a spherical layer of surface molecules makes it possible to relate these quantities. In so doing, it is convenient to prescribe a minimum number of bonds, i.e., two, to the effective surface molecules. In such model, the lightest clusters consist solely of the surface molecules. This allows one to interpolate between the cases of a light and large cluster [Eqs. (1) and (3)] in the following way:

$$\Delta\Phi_c = \Sigma - (g-1)T\ln\frac{n_1}{n_{1s}}, \tag{4}$$

where Σ is the surface part of the work of cluster formation given by[47]

$$\Sigma = \frac{8\pi\sigma_\infty r_\ell^2}{3(\lambda+2\delta)}(g_0-1). \tag{5}$$

Here, g_0 is the effective number of surface molecules related to g as

$$g_0 = \left(\frac{\lambda}{2}+\delta\right)\left[3(g-g_0)^{2/3}+3\lambda(g-g_0)^{1/3}+\lambda^2\right]. \tag{6}$$

Dependence $g_0(g)$ or $g(g_0)$ can be found from (6). If $g < (\lambda/2+\delta)\lambda^2$ a cluster comprises solely the surface molecules, $g_0 = g$, and the work of cluster formation proves to be proportional to the number of molecules, $\Delta\Phi_c \sim g-1$. In contrast to CNT, the latter implies vanishing of $\Delta\Phi_c$ at some *finite* supersaturation corresponding to a spinodal.

The work of cluster formation (4) can be written in the form (3) if we substitute the size-dependent surface tension

$$\sigma_g = \frac{2\sigma_\infty}{3(\lambda+2\delta)}(g_0-1)g^{-2/3} \tag{7}$$

for σ_∞. It is of interest to compare the dependence (7) with the result of recent study by Julin, Napari, Merikanto, and Vehkamäki[52]. To estimate λ in (6) and (7) for the conditions of Ref. 52, we utilize the fact that the quantity $\delta+\lambda/2$ proved to be almost constant for different substances upon variation of the state parameters[46]. For the conditions of this work (Table I), $\delta+\lambda/2 \simeq 0.773$; hence, if we adopt the estimation $\delta \simeq -0.12$[52] ($\delta \simeq -0.183$ in units of r_ℓ used in this work) we have $\lambda \simeq 1.925$. Figure 1 demonstrates a satisfactory quantitative agreement between the approach developed in this work and the evaluation of the surface tension at the cluster surface of tension based on the results of DFT calculation of the cluster grand potential[53], in particular, an agreement in a sharp increase of σ_g/σ_∞ in the region of small cluster sizes and in the position of maximum of this ratio. Note, however, that we obtain σ_g from the exponent of the cluster size distribution (4) rather than from

the grand potential as in Ref. 53. The dependences similar to (7) were obtained in Refs. 54 and 44. Recently in MD simulation of droplets[55], the Tolman length of negative sign was obtained, whose value corresponds to that reported in Ref. 52. For comparison, we also plot the surface tension obtained from Tolman's equation[32]

$$\sigma_g = \frac{\sigma_\infty}{1 \pm 2\delta g^{-1/3}}, \tag{8}$$

where the positive sign corresponds to a cluster and negative corresponds to a cavity in a liquid. At small cluster sizes, a qualitative disagreement between Tolman's σ_g and above-mentioned calculations is apparent.

Now we pass on to arbitrary size bubbles in a liquid. In CNT[1,2,6], which is relevant for large bubbles, the size distribution of bubbles is written in the form

$$n_g = n_\ell \exp\left(-\frac{\Delta\Phi_b}{T}\right), \quad \Delta\Phi_b = 4\pi\sigma_\infty r_\ell^2 g^{2/3} + \frac{p_\ell - p_\infty}{n_\ell} g, \tag{9}$$

where $\Delta\Phi_b$ is the work of bubble formation, g is the number of molecules removed from the liquid to form a bubble (bubble equimolar size), p_ℓ is the pressure in the liquid phase, and p_∞ is the saturation pressure. Our purpose is to extend Eq. (9) toward the region of nanobubbles with $g \lesssim 10$. Note that the surface part of the work of bubble formation is the same in Eqs. (3) and (9). This allows one to assume that *extended* distribution of bubbles includes *the same* surface part as extended distribution (4), so that we have to write[48]

$$\Delta\Phi_b = \Sigma + \frac{p_\ell - p_\infty}{n_\ell} g - \Sigma\,|_{g_0=0} = \frac{4\pi}{3}\sigma_\infty r_\ell^2 \left[\frac{2}{\lambda + 2\delta} g_0 + \frac{r_\ell}{\sigma_\infty}(p_\ell - p_\infty) g\right], \tag{10}$$

where Σ is defined by (5) and $\Delta\Phi_b$ satisfies an obvious condition $\Delta\Phi_b\,|_{g=0} = 0$. Hence for clusters and nanobubbles, we employ the same assumption that the surface part of formation work is proportional to the number of surface molecules. Work of formation (10) implies that within the framework of this model, a bubble is represented as a spherical layer of the surface molecules in the bulk of internal molecules over an almost empty sphere (for large nanobubbles, the latter is filled with a vapor). This empty sphere does not necessarily appear in the liquid because small nanobubbles are simply spheres of the surface molecules in the bulk of internal molecules. Here, we preserve similarity between lightest clusters and smallest nanobubbles. Note that we discuss an idealized model designed to describe effectively real nanobubbles in a liquid, which are shapeless rather than spherical (see Sec. V; simulation of bubble nucleation shows that even the large bubbles with $g \sim 10^3$ in the superheated system

take on highly irregular shapes[35]). The difference between $\Delta\Phi_b$'s (9) and (10) defines *the size correction* to CNT determining the rate of bubble nucleation.

Due to geometrical considerations, the relation between g and g_0 for bubbles is different from that for clusters:

$$g_0 = \begin{cases} \left(\frac{\lambda}{2}+\delta\right)(3g_1^{2/3}+3\lambda g_1^{1/3}+\lambda^2), & g \geq g_*, \\ \frac{\lambda+2\delta}{\lambda-2\delta}g, & g < g_*, \end{cases} \tag{11}$$

where $g_1 = g - g_0(\lambda-2\delta)/(\lambda+2\delta)$ and $g_* = (\lambda/2-\delta)\lambda^2$. Obviously for the smallest nanobubbles with typically $g < 10$, we arrive at the same behavior of $\Delta\Phi_b$ as for the lightest clusters

$$\Delta\Phi_b = \frac{4\pi}{3}\sigma_\infty r_\ell^2\left[\frac{2}{\lambda-2\delta}+\frac{r_\ell}{\sigma_\infty}(p_\ell-p_\infty)\right]g, \tag{12}$$

which defines the behavior of a liquid in the vicinity of a spinodal. It is well-known that at great negative pressures, spallation takes place, which is a manifestation of the vicinity of a spinodal. In this model, the spinodal condition is formulated as $\Delta\Phi_b = 0$, which, in view of (12), leads to the spinodal pressure

$$p_\ell = \frac{2}{2\delta-\lambda}\frac{\sigma_\infty}{r_\ell}, \tag{13}$$

where $|p_\ell| \gg p_\infty$ is assumed. It is worth mentioning that formulas (5) and (11) yield a good correlation with experimental data on positronium nanocavities in liquids whose size is of the order of intermolecular distance[56].

For nanobubbles in the Lennard-Jones liquid treated in this work, Tolman's length is assumed to be negative (Table I). This means that the size-dependent surface tension (7), which can be applied to bubbles as well, is less than σ_∞ in the entire range of their sizes (see also Ref. 48). Consequently, the work of nanobubble formation is less than that in CNT. MD simulation of equilibrium small nanobubbles in the Lennard-Jones liquid[45] leads to the opposite result. The surface tension of a microbubble proved to be noticeably greater than σ_∞ at least for $g > 100$, which leads to the positive Tolman length. This positive sign is in accordance with evaluation of the surface tension for clusters (droplets), which in the same study was found to be less than σ_∞. The latter contradicts the results of above-mentioned studies[52,55] and the estimate of δ in Ref. 51. In addition, it is necessary to assume a correction decreasing the surface tension (negative δ) to bring a theory in accordance with MD simulation of a liquid spall[41].

Note that the preexponential factor in distribution (9) of CNT is set to n_ℓ mainly due to dimensionality considerations. As it will be shown in the next Section, knowledge on the smallest nanobubble size distribution makes it possible to evaluate it.

III. THE PRE-EXPONENTIAL FACTOR FOR BUBBLE DISTRIBUTION

We formulate now a very simple model of nanobubbles based on the discussion of the previous Section. A liquid is represented as a bulk of internal molecules with the number of bonds distributed about some typical value and a small admixture of the surface molecules with the lowered number of bonds. The surface molecules are grouped in "clusters", monomers of such bond-deficient molecules being the smallest ones. We assume further that the total number of molecules removed from the liquid to form such nanobubbles is negligibly small as compared to the total number of molecules in the system, so that the number density of internal molecules is close to n_ℓ. We also assume that the total volume occupied by the surface molecules is sufficiently small to be below the percolation threshold. This allows one to treat individual clusterlike regions of lowered local density. In other terms, we have formulated a "two-phase" model, which effectively represents local density fluctuations as spontaneously emerging lower-density phase regions in the mother phase of higher density. Introduced model implies that within each "phase", the molecule number densities are constants *identically*. Therefore, fluctuations of the total number of liquid molecules are defined by fluctuations of the number of molecules removed from the liquid to form given set of nanobubbles. Obviously, the model implies *asymmetry* of density fluctuations.

When applied to nanobubbles, the form of classical bubble size distribution, $n_g = n_\ell \exp(-\Delta\Phi_b/T)$, should be refined. The first improvement arises from the fact that g cannot be treated as an integer because the densities of two "phases" are of the same order of magnitude [typically, the density is $(\lambda + 2\delta)n_\ell/2\lambda \sim n_\ell/3$ for the surface molecules[51]], in contrast to the case of clusters in a vapor, where the liquid and vapor number densities differ by two or three orders of magnitude. Therefore, we have to introduce the instant numbers of bubbles with sizes ranging from g to $g + dg$ in the volume V, $N_g dg$, so that its average is $\langle N_g \rangle\, dg = n_g V dg$, where the corresponding size distribution density is $n_g = C n_\ell \exp(-\Delta\Phi_b/T)$ and C is a correction factor.

In contrast to clusters in a vapor, we cannot define C by the "boundary condition"

$n_g \to n_1$ as $g \to 1$ (n_1 is the monomer number density) because in the case of nanobubbles, a physically meaningful quantity is a number of nanobubbles with sizes less than g, $VCn_\ell \int_0^g \exp(-\Delta\Phi_b/T)\, dg$, which vanishes as $g \to 0$. Hence, we have to consider a higher-order quantity, e.g., the variance of total number of molecules N in the volume V, $\langle(\Delta N)^2\rangle$, where angular brackets denote averaging. This quantity can be calculated on the basis of nanobubble size distribution. Since the fluctuation of N is

$$\Delta N = N - \langle N\rangle = V\int_0^\infty g n_g\, dg - \int_0^\infty g N_g\, dg, \tag{14}$$

we have

$$\left\langle(\Delta N)^2\right\rangle = \int_0^\infty\int_0^\infty g_1 g_2 \left\langle (N_{g_1} - n_{g_1}V)(N_{g_2} - n_{g_2}V)\right\rangle\, dg_1 dg_2. \tag{15}$$

Then we employ an obvious assumption of the absence of interaction and, therefore, correlation between the nanobubbles, which is valid if their effect on the average number density of a liquid is sufficiently small: $\langle(N_g - n_g V)(N_{g+g'} - n_{g+g'}V)\rangle = \langle(N_g - n_g V)^2\rangle\, \delta(g')$, where $\delta(g)$ is the delta function. With the same assumption, the statistical distribution of N_g is Gaussian, therefore, its variance is equal to its average, $\langle(N_g - n_g V)^2\rangle = \langle N_g\rangle = n_g V$. Hence, we can rewrite (15) as

$$\left\langle(\Delta N)^2\right\rangle = \int_0^\infty g^2 \left\langle(N_g - n_g V)^2\right\rangle\, dg = V\int_0^\infty g^2 n_g\, dg. \tag{16}$$

In fact, the assumption which leads to (15) means that we treat a weak solution of bubbles in a liquid. This model was employed in Ref. 24, where the probability to find a critical bubble whose volume and pressure inside can fluctuate is calculated.

Assuming that solely small nanobubbles with $g < g_*$ contribute to sought variance of N, we substitute the size distribution of nanobubbles with $\Delta\Phi_b$ (12) rewritten as

$$n_g = Cn_\ell \exp(-\alpha g), \quad \alpha = \frac{4\pi}{3}\frac{\sigma_\infty r_\ell^2}{T}\left[\frac{2}{\lambda - 2\delta} + \frac{r_\ell}{\sigma_\infty}(p_\ell - p_\infty)\right] \tag{17}$$

in Eq. (16) to derive $\langle(\Delta N)^2\rangle = 2CVn_\ell\alpha^{-3}$.

On the other hand, the quantity $\langle(\Delta N)^2\rangle$ can be estimated on the basis of liquid equation of state using well-known formula[57] $\langle(\Delta N)^2\rangle = -T(N/V)^2(\partial V/\partial p_\ell)_T$, whence it follows that

$$C = -\frac{\alpha^3 T}{2}\left(\frac{\partial \ln V}{\partial p_\ell}\right)_T. \tag{18}$$

The equation of state for the Lennard-Jones fluid is elaborate[58–61] but we will employ the simplest one, the van der Waals equation

$$p = \frac{Tn}{1 - bn} - an^2, \tag{19}$$

where $n = N/V$ and a and b are the parameters, to evaluate the derivative in (18). To ensure a correct account of the binodal, we assume a and b to satisfy the Maxwell equal-area rule. If we confine ourselves to the bimodal vicinity then the conditions $|p_\ell|\,, p_\infty \ll n_\ell T$ are satisfied, and we obtain approximately $a \simeq T/x_s n_{\ell s}$, $b = (1 - x_s)/n_{\ell s}$, where $n_{\ell s}$ is the number density of molecules in the liquid phase at saturation, $x_s = 1 - bn_{\ell s}$ is a solution of the equation

$$x_s \ln \omega x_s = -1, \tag{20}$$

where ω is the ratio of the vapor and liquid densities at the saturation curve. Because $\omega \ll 1$, $x_s \ll 1$ for most substances (Table I). Calculation of the derivative in (18) yields

$$C \simeq \frac{1}{2}\alpha^3 D(N), \quad D(N) \equiv \frac{\langle (\Delta N)^2 \rangle}{N} = \frac{n_{\ell s} x_s x^2}{n_{\ell s} x_s - 2n_\ell x^2}, \tag{21}$$

where $x = 1 - bn_\ell = 1 - (n_\ell/n_{\ell s})(1 - x_s)$. At the saturation curve, $x = x_s$ and $D(N) = x_s^2/(1 - 2x_s) \simeq x_s^2$, and we arrive at a very simple estimation $C \simeq \alpha^3 x_s^2/2$. Table I presents the results of estimations of main nanobubble parameters for the substances, for which a set of necessary data is available. In contrast to CNT, C can vary by four orders of magnitude for different substances. This can have an appreciable effect on the number density of nanobubbles, which is written explicitly by incorporation of Eqs. (10) and (21)

$$n_g = \frac{1}{2} n_\ell \alpha^3 D(N) \exp\left\{ \frac{4\pi}{3} \sigma_\infty r_\ell^2 \left[\frac{2}{\lambda + 2\delta} g_0 + \frac{r_\ell}{\sigma_\infty} (p_\ell - p_\infty) g \right] \right\}. \tag{22}$$

Using Eqs. (17) and (21) one can calculate the equivalent number of molecules removed from the liquid in unit volume at the saturation curve

$$\chi = \int_0^\infty g n_g \, dg = \frac{\alpha}{2} \frac{x_s^2}{1 - 2x_s}. \tag{23}$$

The number of molecules removed from the liquid to form an ensemble of nanobubbles at equilibrium (23) is in fact small (see Table I), which validates our assumption. The quantity α^{-1} represents a typical size of nanobubbles that contribute to the total volume of nanobubbles in a liquid. As evident from Table I, this size is very small, it varies by two

orders of magnitude for different substances but $\alpha^{-1} \lesssim 1$. At the same time, we see that $\alpha g_* \gg 1$, which validates the use of distribution (17) for the smallest nanobubbles instead of the general size distribution (22).

IV. MD SIMULATION PROCEDURE

We have performed a MD simulation to verify the model bubble size distribution (22). A droplet of the Lennard–Jones fluid with a long-range interaction surrounded by gas was chosen as a simulation ensemble. The particles interact via the potential

$$u(r) = -\frac{\gamma}{r} + \begin{cases} v(r) - v(r_c), & r \le r_c, \\ 0, & r > r_c, \end{cases} \qquad v(r) = 4\varepsilon\left(\frac{a^{12}}{r^{12}} - \frac{a^6}{r^6}\right), \tag{24}$$

where r is the interparticle distance, γ is the long-range coupling constant, $r_c = 2.5a$ is the cutoff radius, ε is the well depth, and a is the length scale. In what follows, we use the MD units: $\tau_0 = a\sqrt{M/24\varepsilon}$, for the time ($M$ is the particle mass); a, for the distance; a^{-3}, for the particle density; ε, for the energy; ε/a^3, for the pressure. Also, we use the energy units for temperature T; in this study, simulation is performed at the fixed temperature $T = 0.75$ (89.6 K for $\varepsilon = 119.4$ K and $a = 3.4 \times 10^{-8}$ cm).

MD simulation procedure based on the (P, T)-ensemble method is discussed in detail in Refs. 49 and 50. It makes it possible to simulate an open system with predetermined pressure and temperature but fluctuating energy and number of particles. The latter is especially important because it makes it possible to estimate independently the fluctuation of the number of particles in a fixed ensemble volume and relate it to determined size distribution of the nanobubbles. Utilization of this ensemble ensures an easy and effective control over the pressure inside a simulated droplet. In contrast to the NVT-ensemble generally used for simulation of bubbles in a liquid, the pressure changes simultaneously with the change of the long-range coupling constant, and this change requires no time for equilibration. Indeed, the long-range part of interaction potential (24) stipulates an additional pressure in the bulk of a droplet

$$p_\ell(r) - p_{\text{vp}} = \frac{2\pi}{3}\gamma n_\ell^2 R_d^2\left(1 - \frac{r^2}{R_d^2}\right) + \frac{2\sigma_\infty}{R_d}, \tag{25}$$

where $p_{\rm vp} \approx n_1 T$ is the pressure of the vapor that surrounds a droplet, R_d is the droplet radius, r is the distance from the droplet center of mass, and the third term is the Laplace pressure. Under conditions specified above, $n_\ell = 0.758$, $\sigma_\infty = 0.483$[62], and $R_d = 21.1$. Note that in this work, we use σ_∞ calculated for the Lennard-Jones potential without a long-range component. It was shown in Ref. 49 that the long-range component of interparticle potential (24) induces a field, which has no effect on the surface tension of a flat interface even for strong fields. This justifies our choice of σ_∞.

For typical value $n_1 \approx 0.013$, $p_{\rm vp} \sim p_\infty \ll 2\sigma_\infty/R_d$ and $2r_\ell/R_d \ll 2/(\lambda - 2\delta)$, $(8\pi/3)(\sigma_\infty g_* r_\ell^3/TR_d) < 1$. This allows one to neglect p_∞ and the Laplace pressure in Eq. (17) and to write approximately $p_\ell \simeq (2\pi/3)\gamma n_\ell^2 R_d^2$. For the reduced pressure $p = (p_\ell - p_\infty) r_\ell/\sigma_\infty = 0$, nanobubbles were searched for in the bulk of a droplet truncated by a sphere with the radius $R_{\rm tr} = 14$ to eliminate the effect of the droplet surface. For $p = -0.16$ and 0.8, we confined ourselves to a sphere of the radius $R_{\rm tr} = 9$. Within this sphere, the pressure changes by less than 20%. Note that for $p = 0.8$, both terms in square brackets in Eq. (17) are close, and the pressure variation inside the sphere of truncation cannot change the nanobubble distribution considerably at $g < g_*$.

Our purpose will be investigation of the smallest nanobubbles with $g \lesssim g_*$. According to the concept of our model such nanobubbles include no obvious empty spaces. Therefore, a problem arises how to identify them in a bulk liquid. We propose an identification method based on the analysis of the local distribution over the number of bonds. Albeit this way of nanobubble identification may be neither unique nor the most efficient one, to our knowledge, no relevant method was reported in the literature. On the other hand, it is shown below that proposed method results in a satisfactory correlation with the theory. By definition, a particle has a bond if it has a neighbor at the distance less than r_b. Correspondingly, the number of bonds for given particle is the number of neighboring particles within a sphere with the radius r_b. This definition descends from Stillinger's definition of a cluster[63]: a particle pertains to the cluster if it has at least one bond with a particle pertaining to the same cluster. It was demonstrated in Ref. 64 that for specified temperature, there exists some value of r_b, for which the number of Stillinger particles is equal to the number defined by the cluster equimolar size. In addition in the neighborhood of this value, both numbers (or sizes) are independent of r_b. Thus, this quantity defines a characteristic correlation scale, e.g., for $T = 0.75$, $r_b = 1.65$. This scale is close to the distance to the first minimum of

the radial distribution function, which was proposed to be used as a characteristic value in Ref. 63. We will adopt the above-mentioned value of this parameter in what follows. One can suppose that a nanobubble is a region in space where the concentration of particles with the number of bonds b lower than b_ℓ, the average one for treated liquid, is enhanced. In other terms, a nanobubble must be marked by particles with a small number of bonds. In what follows, we will term them the bond-deficient particles. Since we believe that a nanobubble is a single correlated formation, the distance between these bond-deficient particles must be less than r_b. Thus, we expect the bond-deficient particles to clusterize in a liquid and apply to them the definition of Stillinger cluster with r_b specified above. The number of bond-deficient particles that comprises such bond-deficient cluster (BDC) will be referred to as the BDC size k. BDC particles mark the spatial region where a nanobubble resides. By definition, for a bond-deficient particle, $b < b_{\max}$. Selection of bond-deficient particles depends crucially on the choice of the maximum number of bonds $b_{\max}$, which depends on the system parameters. Obviously, if $b_{\max}$ was too low, a considerable part of nanobubbles would be missed. If it was too high, the total volume of nanobubbles detected in such a way would exceed ca. 1/3 of the system volume and, therefore, the percolation threshold. Thus, system-spanning BDC's emerge. Manifestation of this fact in simulation would be an inappropriate dependence of BDC size distribution on the system volume. Hence, we have to choose $b_{\max}$ from competitive considerations, namely, we set it to the maximum value below the percolation threshold. As will be seen, $b_{\max}$ increases with increasing b_ℓ when the pressure is increased.

Each nanobubble can be characterized by its "instantaneous" quantities, the size k and molecular size g_v [see Eq. (26)]. Averaging the latter yields the equimolar size $g(k)$, which can be determined from MD simulation. We will introduce the definition of a nanobubble as follows. Let $R_{\rm cm}$ be the largest distance between the center of mass of bond-deficient particles that form BDC and a bond-deficient particle pertaining to this BDC. Then the radius of a nanobubble is defined as $R_v = (R_{\rm cm}^2 + r_b^2)^{1/2}$. Selected formula ensures a fast convergence to the limits of small and large k 's. In the first limit, $R_v \simeq r_b$ to include all correlated particles, and in the second one, $R_v \simeq r_b$ to minimize possible nanobubble overlapping. We note again that a nanobubble is a shapeless nonspherical formation, so that R_v is a conventional quantity, and the sphere with this radius also includes particles

that are not bond-deficient (see Sec. V). The nanobubble equimolar size is then

$$g = \left\langle \frac{4\pi}{3} n_\ell R_v^3 - g_v \right\rangle, \tag{26}$$

where g_v is the total number of particles within a distance R_v from BDC center of mass and angular brackets denote averaging. For BDC's consisting of a single bond-deficient particle, it is essential to avoid a hard effect of the particle correlation appearing in the radial distribution function on g_v. With this purpose, the BDC center of mass was placed at the half-distance between a single bond-deficient particle and its nearest neighbor. Another quantity, which can be obtained from MD simulation as well, is the size distribution of BDC's f_k. It can be easily related to the theoretical quantity n_g. In fact, the number density of BDC's with the sizes ranging from k to $k+1$, f_k, must be close to the number density of nanobubbles with the sizes ranging from g to $g+dg$, $n_g dg$. Since $dg = (dg/dk)\, dk$, we have $n_g \simeq f_k (dg/dk)^{-1}$. Similarly, one can determine from simulation the average bond deficiency of a nanobubble with the equimolar size g

$$\Delta B_g = \left\langle \frac{4\pi}{3} n_\ell b_\ell R_v^3 - \sum_{i=1}^{g_v} b_i \right\rangle, \tag{27}$$

where b_i is the number of bonds for the i th particle. MD estimation by Eq. (27) can be compared with a theoretical one. According to the theory developed in Sections II and III, the distributions of both the clusters and the nanobubbles are determined by the numbers of internal and surface particles that constitute them. Since the surface particles are bond-deficient, one can expect the bond deficiency ΔB_g to be the most important characteristic of a nanobubble. Therefore, it is of interest to estimate this quantity. If we limit ourselves to the nanobubbles with $g < g_*$, ΔB_g is defined solely by the number of surface particles. The effective surface particles introduced in this model to interpolate from a microscopic to macroscopic bubbles have two bonds. Hence, $\Delta B_g = (4\pi/3) R_v^3 n_\ell b_\ell - 2g_0 = b_\ell \eta g_0 - 2g_0$, where $\eta = 2\lambda/(\lambda + 2\delta)$ is the ratio of number densities of internal and surface particles. Since $g_0 = (\lambda + 2\delta)/(\lambda - 2\delta) g$, we arrive at the dependence

$$\Delta B_g = 2 \frac{(b_\ell - 1)\lambda - 2\delta}{\lambda - 2\delta} g, \tag{28}$$

which is linear in g and independent of the pressure.

MD simulation of an initialized liquid droplet containing 30000 particles on the average surrounded by a saturated vapor at stabilized equilibrium[49] in a simulation cell with the

radius of 42 MD units was performed for the bulk pressures $p = -0.16$, 0.0 and 0.8. Note that the pressure $p = -0.16$ is slightly below the fission threshold for a droplet ($p = -0.8$ would be slightly above the liquid spall threshold); $p = 0.0$ corresponds approximately to the saturation curve. Each simulation comprised two runs with the total MD time of 2.5×10^4 that ensures reasonable accuracy of the nanobubble size distributions. The coordinates of all particles were stored every 25 time units. Subsequent processing of the data included BDC recognition based on the analysis of particle coordinates according to BDC definition discussed above. In so doing, only the particles inside the sphere with the radius $R_{\rm tr}$ were analyzed; BDC's intercepting this sphere were ignored (involved decrease of the system volume was negligibly small). Then all BDC characteristics of interest including their size distribution were calculated along with parameters of the whole system such as n_ℓ and b_ℓ.

V. RESULTS AND DISCUSSION

Snapshots of typical particle configurations are shown in Figs. 2 and 3. Figure 2 illustrates our notion of nanobubbles as spatial regions of enlarged distances between the neighboring particles. Obviously, there could be no well-defined positioning of a nanobubble if the size of empty core inside it is comparable with the interparticle length. At the same time, it is impossible to delimit the nanobubble with an evident core (bubble) and without it (cluster of bond-deficient particles). Figure 2 corresponds to a transitional case, $g \gtrsim g_*$, and onset of an empty core is visible. Note that a nanobubble that contains an empty space with $g_1 = 1$ [cf. Eq. (11)] includes $g_0 \sim 10$ particles independently of the substance. Thus, for mercury, water, and the Lennard-Jones fluid, $g_0 = 6$, 10, and 12, respectively; g is of the same order of magnitude. It is seen that particular BDC finds itself inside a sphere with the radius R_v, and the particles inside this sphere look like a soft matter with the minimum number of bonds. However, according to Ref. 51 the average number of bonds for surface particles increases almost linearly with the decrease of $g^{-1/3}$, i.e., with the decrease of curvature radius. For a negative curvature radius (nanobubble), one can expect further increase of this quantity. Thus, bond-deficient (soft matter) particles inside nanobubbles must have greater number of bonds than similar particles comprising the lightest clusters. In Fig. 3, all particles but the bond-deficient ones are not shown to visualize BDC's. Light clusters in the vapor at the same temperature and saturation pressure simulated using the same procedure are shown

for comparison. It is seen that at negative pressure, BDC's comprise particles with less number of nearest neighbors. A similarity between BDC's and clusters is noteworthy; all of them are shapeless formations. Since their size is in the transitional region, no apparent core (empty or solid) is visible. The average distance between particles is noticeably larger than the average interparticle distance in a bulk liquid and is close in Fig. 3(a) and (b). This validates the application of a bond length of r_b for the definition of a BDC. It is interesting that for BDC's, the most representative numbers $b = 9$ and 10 correspond to $b_\ell - b \approx 3$ and 4 for clusters. Clusters seem to be more compact and comprise particles with greater b possibly because for them, a dense core must emerge at lower g [in fact, $g_* > (\lambda/2 + \delta)\lambda^2$ for negative δ; cf. Eqs. (6) and (11)].

Size distributions of BDC's recognized for different $b_{\max}$ are shown in Fig. 4. It is seen that the BDC number density increases with the increase of $b_{\max}$. However at $b_{\max} = 12$, we have $f_k \sim k^{-2}$, consequently, the series $\sum_{k=1}^{\infty} k f_k$ equal to the total number of bond-deficient particles would diverge in the limit of infinite volume. Manifestation of this fact is a noticeable change of this distribution upon variation of $R_{\rm tr}$, while for $b_{\max} < 12$, the distributions are independent of $R_{\rm tr}$. A physical reason for such behavior is illustrated by Table II. The quantity v overestimates somewhat the volume fraction occupied by the bond-deficient particles because it does not account for clusterization of these particles but it still provides a satisfactory estimate due to the fact that $\chi \ll 1$. Table II is indicative of the fact that as $b_{\max}$ is increased, v approaches the percolation threshold ($\sim 1/3$), which is trespassed at $b_{\max} > 11$. As a result, the fraction of monomer BDC's with $k = 1$ ("compressibility factor") drops sharply from unity to small numbers. This means formation of very large system-spanning BDC's with the characteristic size $R_v \sim R_{\rm tr}$. Such system partitioning is obviously senseless, and we are led to the conclusion that for $p = 0$, the optimum number of bonds is $b_{\max} = 11$. This number was used for a test calculation of the BDC size distribution with random numbers of bonds. With this purpose, numbers of bonds specific for the bond-deficient particles were shuffled, which modeled the random distribution. Resulting distribution distorted in such a way (Fig. 4) reveals a considerably faster vanishing than the original one (they differ by more than two orders of magnitude at $k = 10$), which is the evidence of a tendency for the bond-deficient particles to clusterize inside nanobubbles.

Figure 5 presents the results of calculation of the nanobubble equimolar sizes using Eq. (26). Note that the dependence $g(k)$ is not much different from a linear one with

the slope slightly decreasing as $b_{\max}$ is increased; at $b_{\max} = 11$, $g \sim k$. Error bars in the figure demonstrate a level of statistical accuracy (at the level of confidence of 0.99%) attained in the simulation. At $k > 15$, the accuracy is substantially lowered due to low numbers of BDC's with great k. At the same time, the standard deviation of g is weakly dependent on k and increases with k from 1.7 to 4.2. Hence, for the smallest nanobubbles, fluctuations of instantaneous values of g are of the same order of magnitude as their mean values.

We used the data of Figs. 4 and 5 to calculate the size distribution of nanobubbles $n_g = f_k(dg/dk)^{-1}$ at the equilibrium curve (Fig. 6). At $b_{\max} = 10$, the results of MD simulation essentially underestimate the size distribution due to a low frequency of particles with lower b. At $b_{\max} = 12$, large nanobubble sizes are inaccessible due to the small constant of proportionality between g and k (cf. Fig. 5). For $b_{\max} = 11$, the number densities of nanobubbles nearly reach their maxima and the maximum attainable g is much greater than for $b_{\max} = 12$, therefore, $b_{\max} = 11$ seems to be the optimum one. Note that, due to smallness of the Laplace pressure, this case corresponds to the absence of the long-range interaction component in (24), $\gamma \approx 0$.

In Fig. 6, MD simulation results are compared with theoretical estimations. Rather good correlation between proposed size-corrected theory and simulation is noteworthy. Yet CNT still provides a reasonable agreement within less than two orders of magnitude. This is due to cancellation of two factors; namely, neglect of the correction factor $C \approx 0.01$ and missed correction for the size in CNT. However, our simulation agrees noticeably better in slope with present theory than with CNT. The same applies to the CNT with the Tolman's size correction, when σ_∞ in (9) is substituted for σ_g (8). The region of vanishing g is the most uncertain for both the simulation and theory. It is seen that the nanobubble concentrations are almost independent of $b_{\max}$ in this region, and the data scatter increases as $g \to 0$.

It is of interest to compare obtained nanobubble size distribution with the equilibrium distribution of cavities determined in Ref. 44. It is important to note the difference between the cavities defined as spheres containing no molecules[44] and nanobubbles treated in this work, which are implied to be microscopic density fluctuations. As the radius of a cavity vanishes, the probability to find an empty cavity tends to unity, which makes it possible to normalize the volume occupation probability, which is nearly Gaussian in this size region. We recall that in our case, the number of nanobubbles with sizes less than g is not Gaussian and it vanishes as $g \to 0$; thus, normalization of the size distribution requires additional

considerations (see Sec. III). Albeit n_g and the volume occupation probability[44] are in principle different quantities, they have much in common. Obviously, these distributions have the same macroscopic limit and follow the same non-Gaussian exponential dependence. For cavities, pronounced deviation from the Gaussian dependence takes place already at the cavity radius of $1.5a$. The same trend of void clusterization is seen in Fig. 4, where at the same length scale, the concentration of BDC's with random number of bonds is much lower than that of actual BDC's. A similarity between σ_g (7) and the excess chemical potential per unit surface area of the sphere is noteworthy (cf. Fig. 1 and Fig. 2 in Ref. 44). Note a sharp increase of the surface tension at small sizes, existence of its maximum followed by a plateau close to the flat surface value. The length scale over which the attractive interactions in the fluid fluctuate, λ[44], seems to have similar physical meaning as the thickness of the surface layer λr_ℓ in Eq. (1). Lastly, the turnover to a drying regime[44] is similar to the onset of an empty sphere inside a nanobubble (Sec. II) which occurs at $g \sim g_* \sim 10$. The discussion above applies in full to Ref. 43). The distribution of the volume occupation probability is quite similar to that reported in Ref. 44). Note that clusters of molecules are observed only for highly superheated nonequilibrium states of the liquid[43], while the clusters of bond-deficient molecules are found already at equilibrium.

Using Eq. (27) and the data shown in Figs. 4 and 5 we have determined the dependence of ΔB_g on nanobubble equimolar size. Figure 7 demonstrates linearity of this dependence and reveals no apparent dependence on the pressure, in accordance with formula (27). It was noted in Ref. 51 that the internal energy of a cluster connected with the distribution of particles over the number of bonds is fitted by $\delta = -0.175$ and $\lambda = 2.124$. These parameters are somewhat different from those describing the size dependence of cluster chemical potential (they are listed in Table I). One can see that both data sets provide a satisfactory agreement of the theory with the results of MD simulation but the internal energy values improve the agreement noticeably. Thus, the size dependence of bond deficiency for nanobubbles corroborates the main notion of our model.

The choice of $b_{\max}$ is illustrated by Fig. 8 presenting the distribution of bonds for particles pertaining to the bulk liquid inside the sphere with the radius $R_{\rm tr}$ and for the surface particles. The surface particles were sampled directly from the surface of simulated droplet using the method discussed in Ref. 65. The bond distribution functions $F(b)$ are proportional

to the average number of particles with b bonds and normalized so that $\sum_{b=1}^{\infty} F(b) = 1$. All distributions are fitted by the Gauss exponents, which intersect approximately at the point $b_{\max} = 11$ for $p = 0$ (Fig. 8), and this point is close to the distribution half-width. One can see that almost all bond-deficient particles turn out to be the surface ones in accordance with the above-discussed model. As the pressure is increased, the bond distribution is shifted toward greater numbers of bonds (by ca. unity as the pressure is increased from $p = 0$ to 0.8), while the distribution of surface particles is almost independent of p. One can conclude that at $p = 0.8$, the optimum is reached at $b_{\max} = 12$. This choice is justified by Table II, from which one can see that characteristic nanobubble parameters are close to that for $p = 0$ but are shifted by a single bond toward greater value. Figure 9 shows the distributions of nanobubbles over the equimolar size for a compressed liquid. It was plotted in the same way as Fig. 6. It can be seen that Figs. 6 and 9 are qualitatively similar but for a compressed liquid, the number density of nanobubbles decreases with increasing g essentially faster than for a liquid at the equilibrium curve. The maximum nanobubble size in Fig. 6 is higher than in Fig. 9 due to smaller $R_{\rm tr}$ as well: the decrease of this quantity decreases the number of sampled particles from 7100 down to 1700. Note a good correlation between MD simulation and theoretical calculations by formula (22). Again, CNT with and without Tolman's size correction demonstrate worse correlation with the simulation. Note that at $g \to 0$, Eq. (22) yields n_g about three times higher than for $p = 0$ (Fig. 6). Among possible reasons for this fact, we can point out the condition $|p_\ell| / n_\ell T \ll 1$ required in deduction of the correction factor (21), which is violated for $p = 0.8$. Nevertheless, this accuracy is likely to be sufficient for evaluation of the nanobubble number densities.

The nanobubble size distribution was calculated from MD simulation at $p = -0.16$, which is a minimum pressure preserving stability of the simulated droplet[49]. The results are quite similar to those shown in Fig. 6 with higher nanobubble number densities; a good correlation between simulation and theory (22) can be also testified. It would be of interest to investigate the system at the spinodal pressure (13) but the time of droplet fission is of the same order as the characteristic time of liquid spall. One can crudely estimate the spall threshold neglecting the effect of fission dynamics on the pressure in the droplet center and taking into account the increase of the droplet effective radius upon fission, which decreases the absolute value of pressure. In the test simulation, the droplet was first equilibrated at $p = -0.16$ and then the long-range coupling constant was switched so that the pressure reached a spall threshold.

During the simulation, a large nanobubble was registered close to the center of simulation droplet almost immediately after switching the coupling constant if the pressure was less than -0.65, while Eq. (13) yields the spall threshold $p = -0.62$. Despite a considerable error possibly involved in this estimation, such result does not contradict developed theory.

Fluctuations of the number of sampled particles N_s were determined directly from MD simulation data to test the equation of state used in the estimation of correction factor C. For this purpose, the variance of the number of particles inside a sphere with the radius R_{tr} was determined at $p = 0$. Variances determined at different R_{tr} lead to the estimation $\langle(\Delta N_s)^2\rangle / N_s \approx 0.1$, which correlates with the theoretical estimate (21) $D(N_s) \simeq 0.05$. Such accuracy seems to be compatible with that attained in the determination of nanobubble number densities from simulation.

VI. CONCLUSION

We proposed a model of nanobubbles in a liquid that implies a simplified notion of a liquid as regions of lowered density dissolved in a bulk with a constant density. Lowered density regions include particles with low number of bonds similar to that on the top of the interface between liquid and vapor. Such a model can be considered as a limiting case of very small bubbles and is used to construct an extrapolation between nanobubbles with an equimolar size of about a single molecule removed from the liquid and even less up to a macroscopic bubble. This model is aimed at the development of an efficient size correction to the work of nanobubble formation in a liquid in the course of bubble nucleation and thus facilitates a better description of the nucleation process as compared to CNT. This applies primarily to the cases when the embryo of a new phase (a nanobubble) has a dimension commensurate with the intermolecular size in a liquid, which is typical for the state parameters regions in the vicinity of a spinodal, e.g., in the superheated liquid or in the liquid under great negative pressure close to the spall threshold.

To construct such model, we employed a close analogy between small nanobubbles and small clusters, which are also modeled as bound states of molecules with low number of bonds similar to the surface molecules at the liquid–vapor interface. Knowledge of the work of formation for bubbles with an arbitrary size from zero to infinity makes it possible to estimate the pre-exponential constant in the size distribution of bubbles. For this purpose,

we assumed that the fluctuation of the number of particles in a liquid is caused by nanobubble formation in a bulk liquid with a constant (at the microscopic level) density. Sought correction to the classical pre-exponential factor is derived from the relation between thus calculated fluctuations and those based on the fluid equation of state. We used the van der Waals equation combined with the Maxwell equal-area rule as a simplest model equation of state. For different substances, the correction factor differs by orders of magnitude, which is especially important for very small nanobubbles. Estimates show that the most pronounced contribution to the fraction of nanobubbles in a liquid is that from nanobubbles with the equimolar sizes less than unity.

To verify the major concepts of proposed theory, we performed MD simulation of a liquid, in which small nanobubbles were identified and their size distribution was determined. The (P, T)-ensemble method was used for simulation of a macroscopic liquid droplet of particles interacting via the Lennard-Jones plus the long-range potential, and spontaneous formation of nanobubbles at equilibrium inside it was investigated. Selected simulation scheme has an advantage of a simple pressure control in the bulk liquid by the adjustment of the long-range coupling constant, which allowed us to investigate the nanobubble size distributions at different pressures both at the coexistence curve and for strongly compressed equilibrium liquid. We solved a problem of small nanobubbles identification by isolation of the regions with low numbers of bonds per particle, which are associated with the local regions of possible nanobubble residence. In MD simulation, a recognition procedure for the groups of bond-deficient particles was performed for the number of bonds less than some maximum one that results in the total volume fraction of nanobubbles below the nanobubble percolation threshold. With such a choice, obtained nanobubble distribution is independent of the volume of sampling. MD simulation shows that the bond-deficient particles are grouped together in space thus forming bond-deficient clusters. The BDC's are the markers of spatial regions, where nanobubbles reside. Simulation results show that nanobubbles include bond-deficient particles with an admixture of particles with the number of bonds not much different from the average one. The BDC's look quite similar to the light clusters in a vapor. The equimolar sizes of nanobubbles is estimated by inscribing the BDC's in spheres and counting the number of particles inside them. Thus, one can relate the BDC equimolar size to the number of particles in BDC. For BDC's comprising about ten particles, the standard deviation for such a dependence is much less than the corresponding average size. As a result,

one can plot the nanobubble size distribution as a function of their equimolar size predicted by the theory. The results of simulation demonstrate a reasonably good correspondence with a theory both in the nanobubble size distributions at different pressures in the liquid and in the dependence of the bond deficiency in a nanobubble on its equimolecular size. This correspondence is noticeably better than that with CNT.

In spite of a satisfactory agreement between proposed theory and MD simulation, one can note the following items that should be addressed in future. First, it is not clear from MD simulation that proposed theory is sufficiently correct for nanobubble sizes of unity or smaller because the smallest BDC size $k = 1$ corresponds to the equimolar size $g \sim 1$. Moreover, proposed method of nanobubble identification and numerical determination of g can flaw at such a small value. We recall that this method may not be the best one. Its limitations are connected to the fact that the number of bonds is integer. Therefore, a minimum step is BDC size is unity; one cannot "fine tune" $b_{\max}$. For this reason, MD simulation results cannot reliably resolve the trend of nanobubble size distribution at $g \to 0$, and it is still not clear whether the dependence $n_g(p)\,|_{g=0}$ is decreasing or increasing. For the reasons discussed above, the theory, which leads to a weakly increasing dependence, may also have an insufficient accuracy in this size range.

According to our results listed in Table I the fraction of nanobubbles in a liquid is of the order of several per cent. Ambiguity of this value is due to the following reasons. Apart from validity of formula (22) for $g < 1$, which is not clear, we note that the theory includes no adjustable parameter, and accepted parameters δ and λ may not be the better choice for nanobubbles. For example, note a very small α^{-1} for mercury in Table I. The reason for it is the known metal–dielectric transition of mercury atoms observed both at the flat liquid–vapor interface and in small mercury clusters, which results in an anomalously high surface tension. It is not clear if this transition takes place in nanobubbles; accordingly, if appropriate δ and λ are used in (22). Additionally, the use of van der Waals equation of state can lead to a considerable error, which is most probable for the pressure close to the spall threshold. Also, it is possible that our assumption of a defining role of nanobubble formation for the fluctuations of the number particles in a system is not quite correct. According to Ref. 66 the bond percolation threshold in crystals is reached at the fraction of broken bonds of the order of 0.1, and this level is sometimes believed to be equal to the void fraction in liquids. However, we have shown that it is different from the number of molecules removed

from the liquid (23), at least, in the framework of our definition of this quantity. In any case, we have demonstrated that the effect of nanobubbles on the fluctuations of the particle number is noticeable.

Among other trends of research to be addressed in the future, the following are also worth mentioning. First, it is of certain interest to simulate a liquid spall as close to the spinodal as possible to verify a principal linearity of the dependence (12) leading to the spall threshold (13). Second, development of improved methods of nanobubble identification and measurements of their characteristics, in particular, in NPT- and NVT-ensembles are required. Such investigations would made it possible to increase the reliability of corrections for the size of an embryo in the bubble nucleation theories.

REFERENCES

[1]M. Volmer, *Kinetik der Phasenbildung* (Theodor Steinkopff, Dresden, 1939).

[2]J. Frenkel, *Kinetic Theory of Liquids* (Dover, New York, 1955).

[3]F. Abraham, *Homogeneous nucleation theory* (Academic Press, New York, 1974).

[4]L. Z. Farkas, Phys. Chem. **125**, 236 (1927).

[5]R. Becker and W. Döring, Ann. Phys. **24**, 719 (1935).

[6]Ya. B. Zeldovich, J. Eksp. Teor. Fiz. **12**, 525 (1942).

[7]V. P. Skripov, *Metastable liquids* (Wiley, New York, 1974).

[8]M. Shusser and D. Weihs, Int. J. Multiphase Flow **25**, 1561 (1999).

[9]K. S. Suslick, Fluid Phase Equilibria **247**, 1439 (1990).

[10]C. E. Brennen, *Cavitation and Bubble Dynamics* (Oxford University Press, New York, 1995).

[11]P. Debenedetti, *Metastable Liquids: Concept and Principles* (Princeton University Press, Princeton, NJ, 1996).

[12]A. A. Bogach and A. V. Utkin, J. Appl. Mech. Tech. Phys. **41**, 752 (2000).

[13]A. V. Utkin, V. A. Sosikov, and A. A. Bogach, J. Appl. Mech. Tech. Phys. **44**, 174 (2003).

[14]A. V. Utkin and V. A. Sosikov, J. Appl. Mech. Tech. Phys. **46**, 481 (2005).

[15]F. H. de Rességuiera, L. Signor, A. Dragon, P. Severin, and M. Boustie, J. Appl. Phys. **102**, 073535 (2007).

[16]M. E. Povarnitsyn, T. E. Itina, M. Sentis, K. V. Khishchenko, and P. R. Levashov, Phys. Rev. B **75**, 235414 (2007).

[17]X. C. Zeng and D. W. Oxtoby, J. Chem. Phys. **94**, 4472 (1991).

[18]D. W. Oxtoby, V. Talanquer, and A. Laaksonen, Annu. Rev. Phys. Chem. **46**, 489 (1995).

[19]J. Rowlinson and B. Widom, *Molecular Theory of Capillarity* (Clarendon, Oxford, 1982).

[20]V. I. Kalikmanov, J. Chem. Phys. **124**, 124505 (2006).

[21]D. S. Corti, K. J. Kerr, and K. Torabi, J. Chem. Phys. **135**, 024701 (2011).

[22]S. Ghosh and S. K. Ghosh, J. Chem. Phys. **135**, 124710 (2011).

[23]A. Tröster, M. Oettel, B. Block, P. Virnau, and K. Binder, J. Chem. Phys. **136**, 064709 (2012).

[24]B. V. Deryagin, A. V. Prokhorov, and N. N. Tunitskii, Sov. Phys. JETP **46**, 962 (1977).

[25]N. V. Alekseechkin, J. Phys. Chem. B **116**, 9445 (2012).

[26]T. Yamamoto and S. Ohnishi, Phys. Chem. Chem. Phys. **12**, 1033 (2010).

[27]A. V. Neimark and A. Vishnyakov, J. Chem. Phys. **122**, 234108 (2005).

[28]K. S. Glavatskiy, D. Reguera, and D. Bedeaux, J. Chem. Phys. **138**, 204708 (2013).

[29]H. Reiss, W. K. Kegel, and J. L. Katz, J. Phys. Chem. A **102**, 8548 (1998).

[30]M. Iwamatsu, J. Chem. Phys. **129**, 104508 (2008).

[31]M. J. Uline, K. Torabi, and D. S. Corti, J. Chem. Phys. **133**, 174512 (2010).

[32]R. C. Tolman, J. Chem. Phys. **17**, 333 (1949).

[33]D. S. Corti, P. G. Debenedetti, S. Sastry, and F. H. Stillinger, Phys. Rev. E **55**, 5522 (1997).

[34]I. Kusaka and D. W. Oxtoby, J. Chem. Phys. **111**, 1104 (1999).

[35]S. L. Meadley and F. A. Escobedo, J. Chem. Phys. **137**, 074109 (2012).

[36]S. K. Das and K. Binder, Phys. Rev. Lett. **107**, 235702 (2011).

[37]V. G. Baidakov and S. P. Protsenko, Phys. Rev. Lett. **95**, 015701 (2005).

[38]V. G. Baidakov, K. S. Bobrov, and A. S. Teterin, J. Chem. Phys. **135**, 054512 (2011).

[39]Z.-J. Wang, C. Valeriani, and D. Frenkel, J. Phys. Chem. B **113**, 3776 (2009).

[40]T. T. Bazhirov, G. E. Norman, and V. V. Stegailov, J. Phys. Condens. Matter **20**, 114113 (2008).

[41]A. Yu. Kuksin, G. E. Norman, V. V. Pisarev, V. V. Stegailov, and A. V. Yanilkin, Phys. Rev. B **82**, 174101 (2010).

[42]J. L. F. Abascal, M. A. Gonzalez, J. L. Aragones, and C. Valeriani, J. Chem. Phys. **138**, 084508 (2013).

[43]R. D. Mountain, J. Chem. Phys. **110**, 2109 (1999).

[44]D. M. Huang and D. Chandler, Phys. Rev. E **61**, 1501 (2000).

[45]S. H. Park, J. G. Weng, and C. L. Tien, Int. J. Heat Mass Transfer **44**, 1849 (2001).

[46]D. I. Zhukhovitskii, J. Chem. Phys. **101**, 5076 (1994).

[47]D. I. Zhukhovitskii, J. Chem. Phys. **110**, 7770 (1999).

[48]D. I. Zhukhovitskii, Colloid J. **65**, 480 (2003).

[49]D. I. Zhukhovitskii, J. Chem. Phys. **135**, 044512 (2011).

[50]D. I. Zhukhovitskii, J. Chem. Phys. **103**, 9401 (1995).

[51]D. I. Zhukhovitskii, J. Exp. Theor. Phys. **94**, 336 (2002).

[52]J. Julin, I. Napari, J. Merikanto, and H. Vehkamäki, J. Chem. Phys. **133**, 044704 (2010).

[53]J. Julin, I. Napari, J. Merikanto, and H. Vehkamäki, J. Chem. Phys. **129**, 234506 (2008).

[54]S. M. Thompson, K. E. Gubbins, J. P. R. B. Walton, R. A. R. Chantry, and J. S. Rowlinson, J. Chem. Phys. **81**, 530 (1984).

[55]A. E. van Giessen and E. M. Blokhuis, J. Chem. Phys. **131**, 164705 (2009).

[56]D. I. Zhukhovitskii, Colloid J. **67**, 718 (2005).

[57]L. D. Landau and E. M. Lifshits, *Statistical Physics* (Elsevier, Oxford, 1980).

[58]F. H. Ree, J. Chem. Phys. **73**, 5401 (1980).

[59]A. Lotfi, J. Vrabec, and J. Fischer, Mol. Phys. **76**, 1319 (1992).

[60]J. K. Johnson, J. A. Zollweg, and K. E. Gubbins, Mol. Phys. **78**, 591 (1993).

[61]V. Baidakov, S. Protsenko, and Z. Kozlova, Fluid Phase Equilibria **263**, 55 (2008).

[62]A. E. van Giessen and E. M. Blokhuis, J. Chem. Phys. **116**, 302 (2002).

[63]F. H. Stillinger, Jr., J. Chem. Phys. **38**, 1486 (1963).

[64]D. I. Zhukhovitskii, Russ. J. Phys. Chem. **75**, 1043 (2001).

[65]D. I. Zhukhovitskii, J. Chem. Phys. **125**, 234701 (2006).

[66]J. M. Ziman, *Models of disorder* (Cambridge University Press, Oxford, 1979).

[67]I. K. Kikoin, ed., *Tables of Physical Data. The Handbook* (Atomizdat, Moscow, 1976).

TABLE I. Parameters defining the size distributions of nanobubbles for different substances. For Hg and H_2O, thermodynamic reference data were borrowed from Ref. 67; δ and λ, from Ref. 46; for the Lennard–Jones fluid (LJ), from Ref. 62 and 51, respectively. The values of x_s, g_*, α^{-1}, C, and χ were calculated using formulas (20), (11), (17), (21), and (23) respectively.

Substance	T, K	ω	x_s	δ	λ	g_*	α^{-1}	C	χ
Hg	293	1.83×10^{-9}	0.0430	0.218	1.129	0.442	0.0211	108	0.0479
H_2O	323	8.26×10^{-5}	0.0842	–0.232	1.554	2.44	0.427	0.0547	0.00998
LJ	89.6	1.72×10^{-2}	0.172	–0.420	2.386	9.18	1.292	0.0114	0.0174

TABLE II. Volume fraction occupied by the bond-deficient particles $v = (4\pi/3)r_b^3 \sum_{k=1}^{\infty} k f_k$ and their "compressibility factor" $Z = \sum_{k=1}^{\infty} f_k \left(\sum_{k=1}^{\infty} k f_k \right)^{-1}$ for different maximum bond numbers $b_{\max}$ and pressures p from MD simulation.

p	$b_{\max}$	v	Z
0.0	10	0.0615	0.902
0.0	11	0.366	0.732
0.0	12	1.61	0.373
0.0	13	4.34	0.0595
0.8	11	0.0774	0.929
0.8	12	0.549	0.737
0.8	13	2.38	0.309

FIGURE CAPTIONS

Fig. 1: Reduced size-dependent surface tension as a function of cluster size. Calculation using formula (7) is compared with the DFT result reproduced from Ref. 52 and with Tolman's equation (8).

Fig. 2: Cross section of a typical nanobubble in a bulk of a liquid at $p = -0.16$. Color indicates the number of bonds b for each particle in a sphere with the radius R_v around the nanobubble. Particles inside this sphere not pertaining to the particular BDC ($b > 10$) are labeled by yellow and gray circles; the particles outside the sphere are shown by open circles. Cross section width is 2.

Fig. 3: Snapshots of individual BDC's in a liquid: (a) $p = 0.0$ (first row) and $p = -0.16$ (second row) and (b) clusters in a vapor at the saturation curve. For particular BDC's, color indicates the number of bonds b for each particle, particles with $b \geq 11$ are not shown, and open circles indicate the particles pertaining to BDC's other than the particular ones. For clusters, color indicates the difference $b_\ell - b$ rounded to an integer, open circles indicate the particles not pertaining to particular clusters. Shown are slabs with the widths sufficient to include respective BDC's or clusters.

Fig. 4: Distribution of BDC's over the number of bond-deficient particles for $b_{\max} = 10$, 11, and 12 (listed in the inset). The inverse square dependence and size distribution for the particles with random numbers of bonds are shown for reference.

Fig. 5: Equimolar sizes of the nanobubbles marked by BDC's comprising k bond-deficient particles for different $b_{\max}$ listed in the inset at $p = 0$.

Fig. 6: Distribution of the nanobubbles over their equimolar size for $p = 0$. MD simulations (dots) were performed for $b_{\max} = 10$, 11, and 12 (listed in the inset); horizontal error bars for $b_{\max} = 11$ are the same as vertical error bars in Fig. 5. Lines indicate the size-corrected theory, CNT [formulas (22) and (9), respectively], and CNT with Tolman's correction for size (8).

Fig. 7: Bond deficiency in the nanobubbles as a function of their equimolar size for two pressures. Dots are the results of MD simulation; lines indicate calculations using formula (28) with λ and δ borrowed (1) from Ref. 51 and (2) from Table I.

Fig. 8: Bulk and surface particles distributions over the number of bonds for different pressures.

Fig. 9: Distribution of the nanobubbles over their equimolar size for $p = 0.8$. MD simulations (dots) were performed for $b_{\max} = 11$, 12, and 13. Other notation is the same as in Fig. 6.

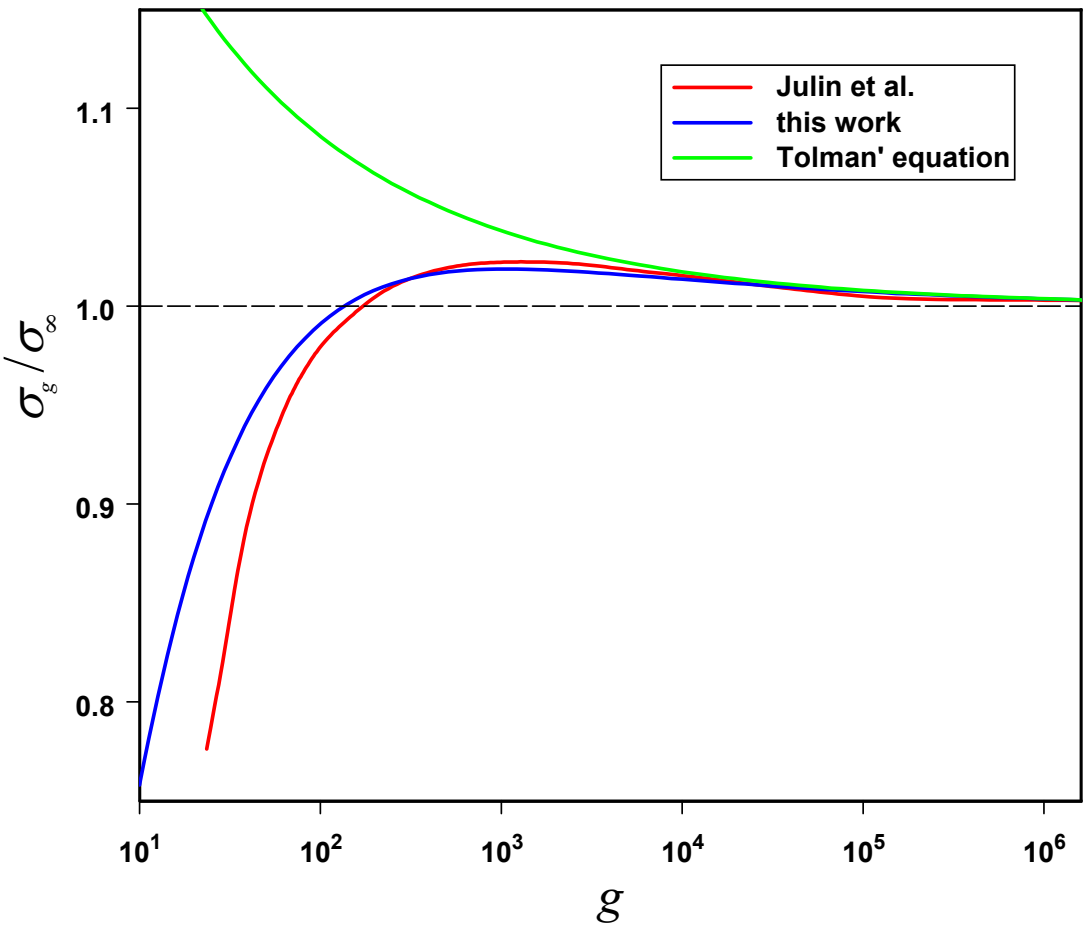
Julin et al.
this work
Tolman' equation
1.1
1.0
0.9
0.8
σ_g/σ_8
10^1
10^2
10^3
10^4
10^5
10^6
g

FIG. 1.

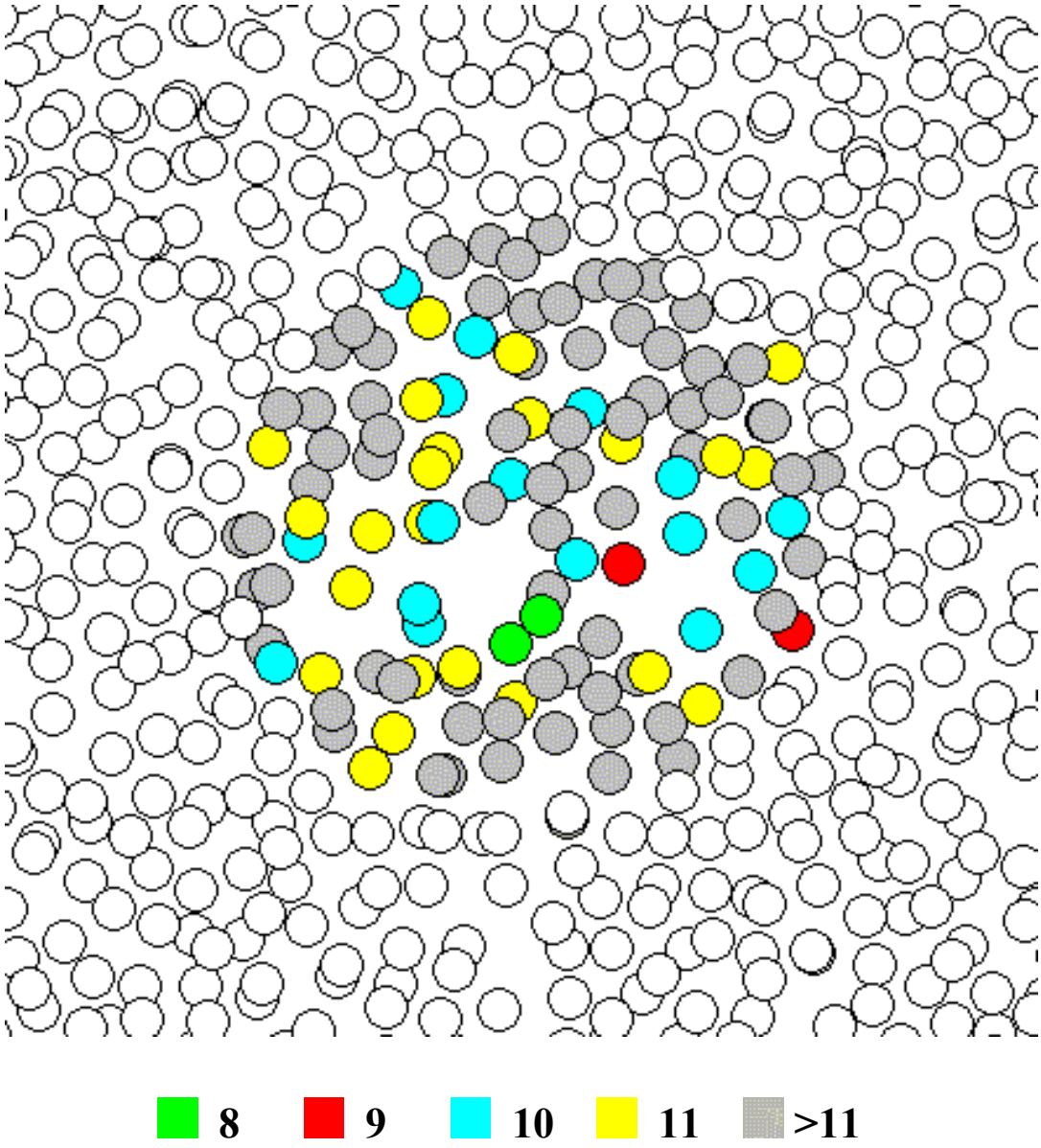

FIG. 2.

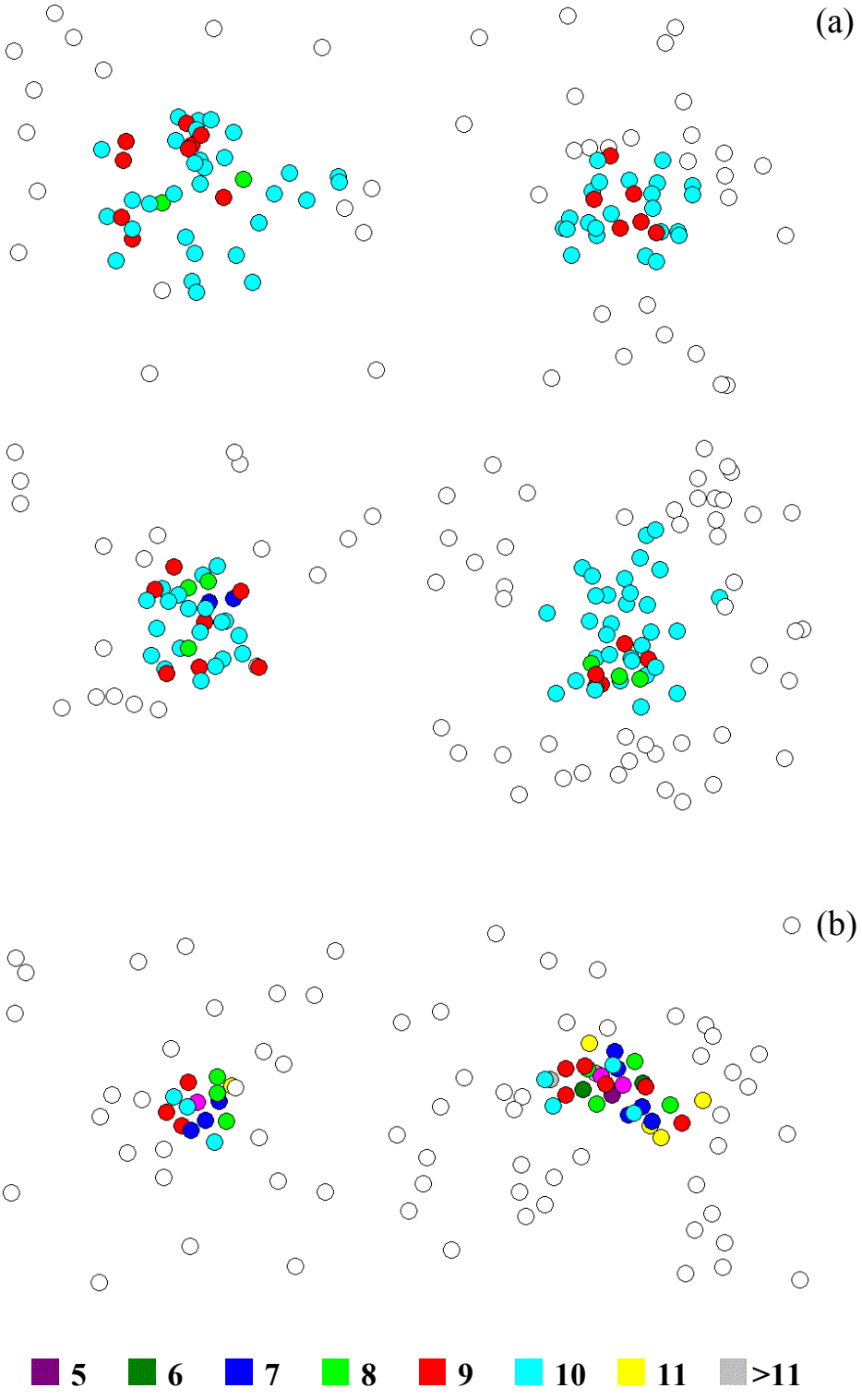

FIG. 3.

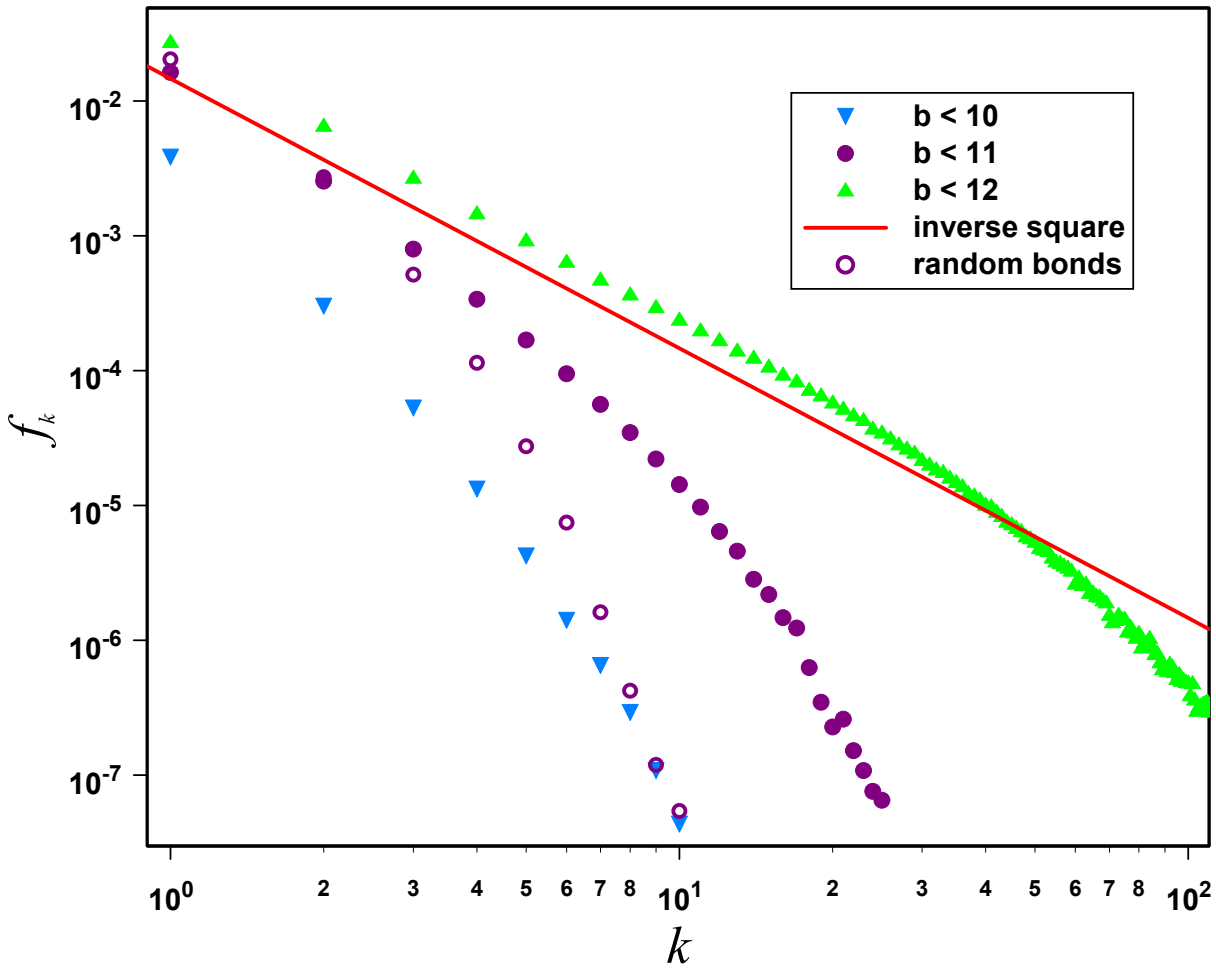
b < 10
b < 11
b < 12
inverse square
random bonds
f_k
k
10^{-2}
10^{-3}
10^{-4}
10^{-5}
10^{-6}
10^{-7}
10^0
10^1
10^2
2
3
4
5
6
7
8

FIG. 4.

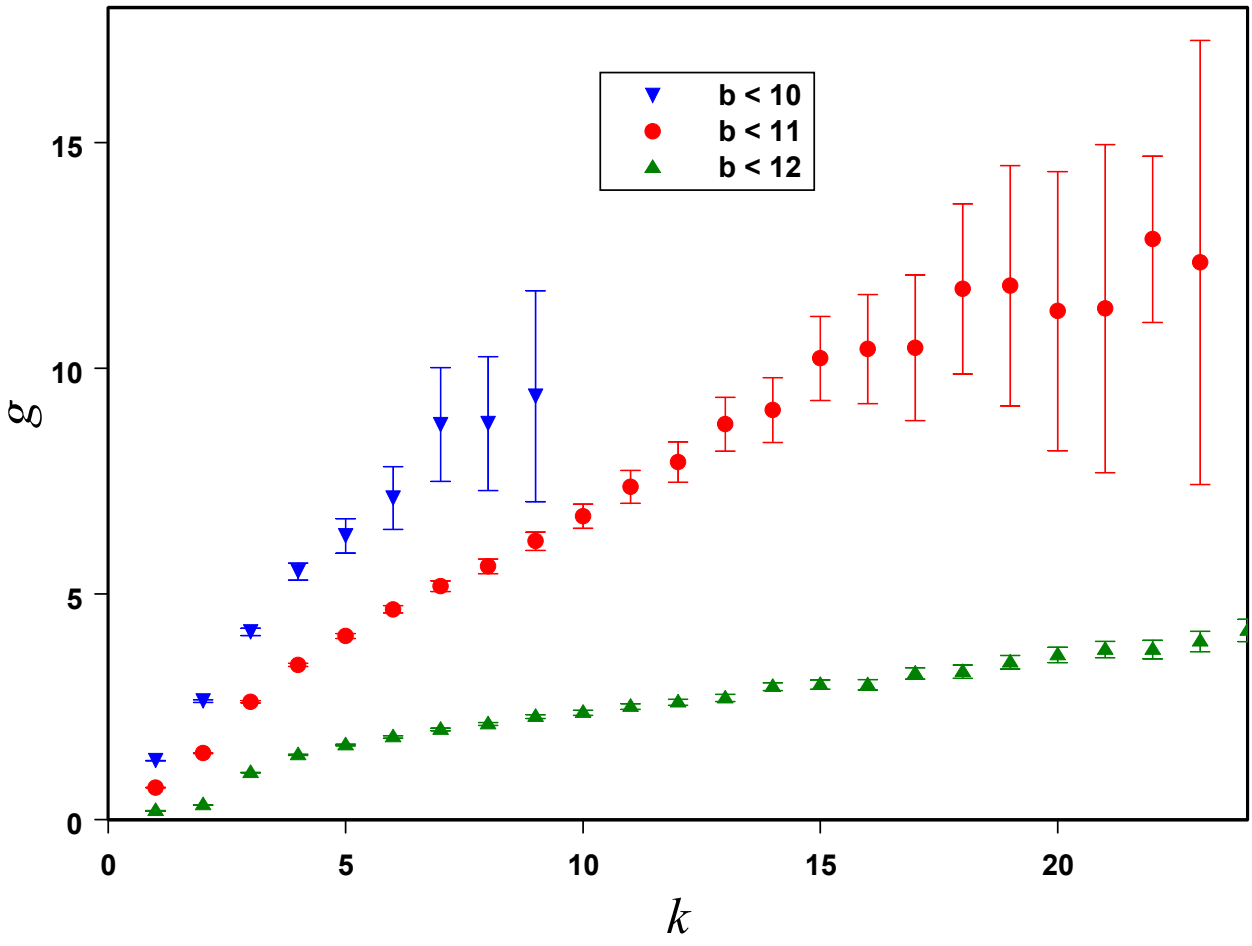

FIG. 5.

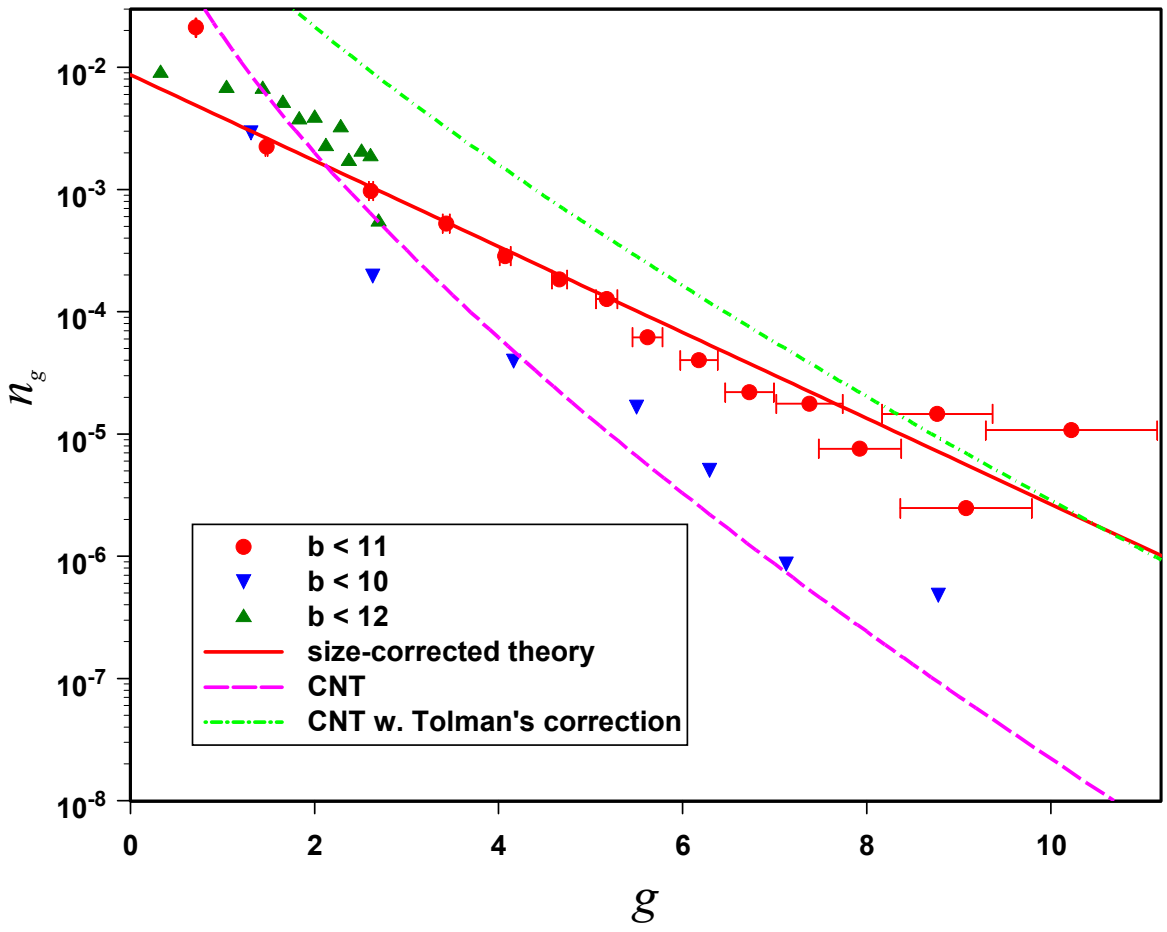
10^{-2}
10^{-3}
10^{-4}
10^{-5}
10^{-6}
10^{-7}
10^{-8}
n_g
0
2
4
6
8
10
g
b < 11
b < 10
b < 12
size-corrected theory
CNT
CNT w. Tolman's correction

FIG. 6.

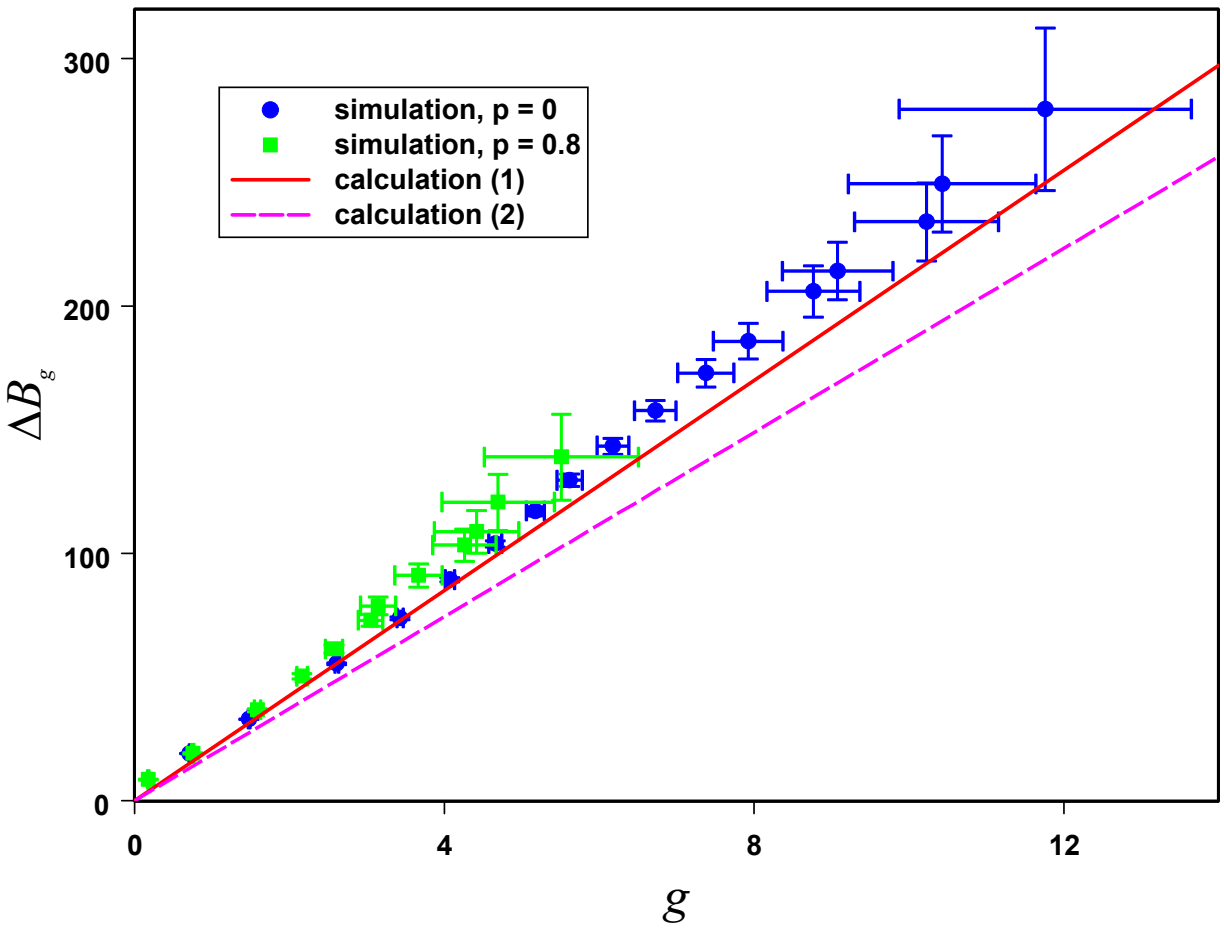
simulation, p = 0
simulation, p = 0.8
calculation (1)
calculation (2)
300
200
100
0
0
4
8
12
ΔB_g
g

FIG. 7.

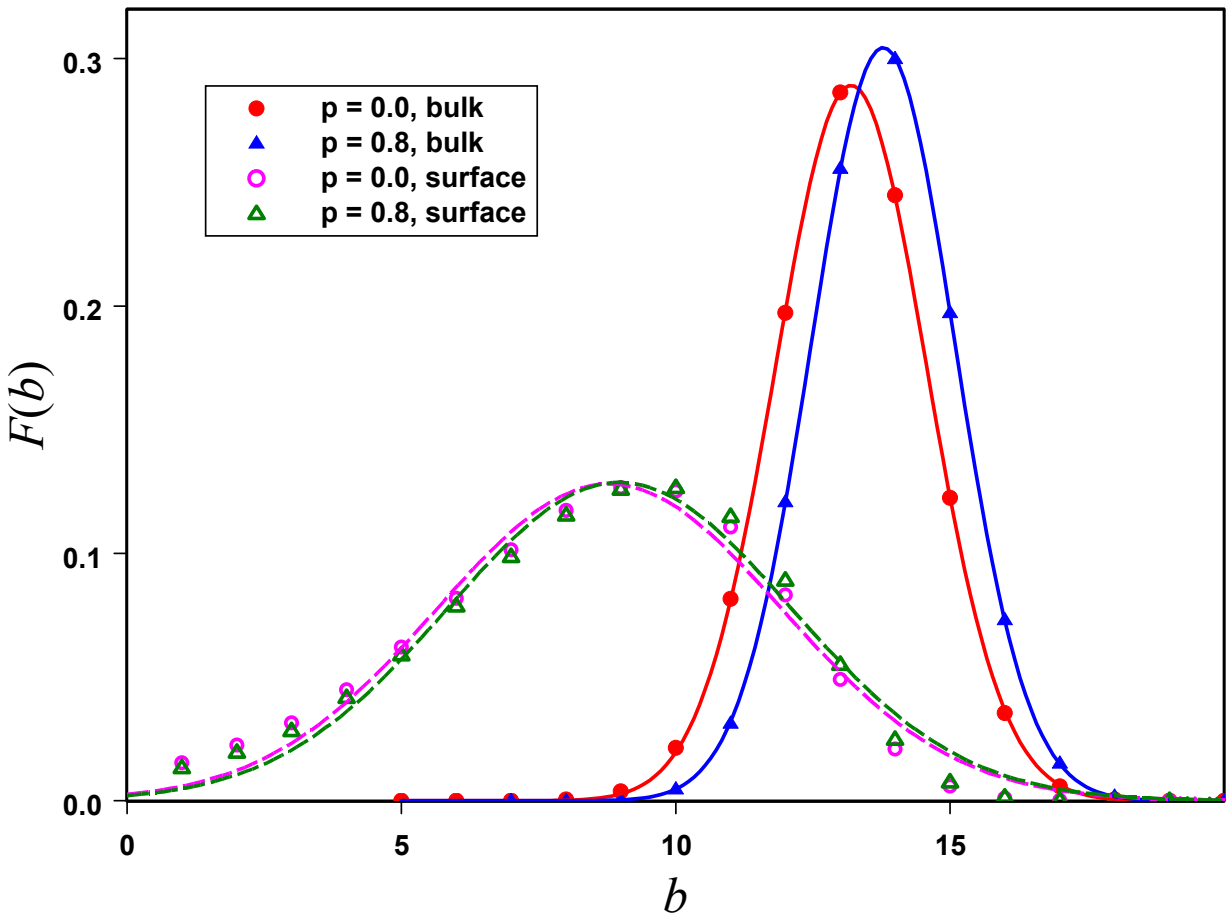
p = 0.0, bulk
p = 0.8, bulk
p = 0.0, surface
p = 0.8, surface
F(b)
b
0.0
0.1
0.2
0.3
0
5
10
15

FIG. 8.

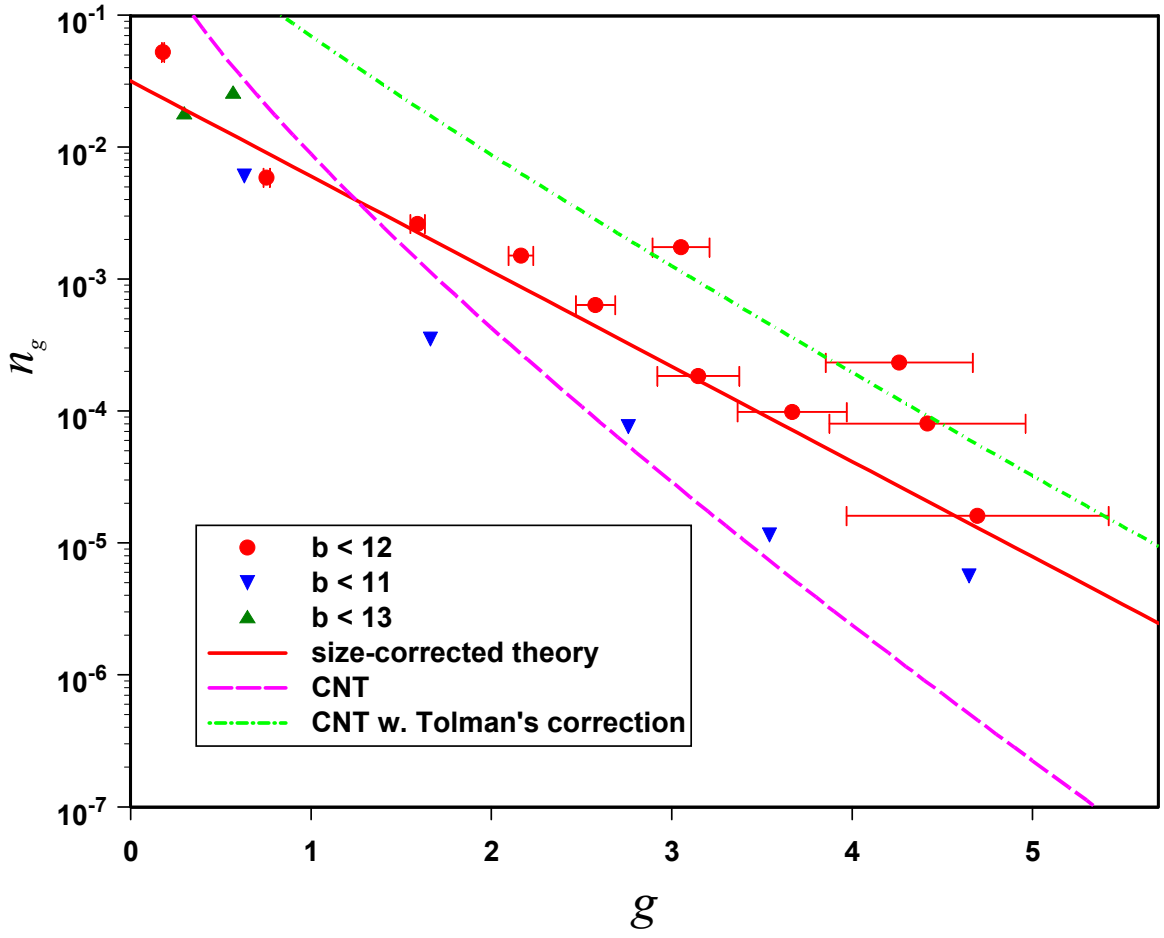
10^{-1}
10^{-2}
10^{-3}
10^{-4}
10^{-5}
10^{-6}
10^{-7}
n_g
0
1
2
3
4
5
g
b < 12
b < 11
b < 13
size-corrected theory
CNT
CNT w. Tolman's correction

FIG. 9.